Available online at www.sciencedirect.com
SCIENCE DIRECT
Journal of Power Sources 155 (2006) 33–46
JOURNAL OF POWER SOURCES
www.elsevier.com/locate/jpowsour

# Ethylene glycol electrooxidation on carbon supported Pt, PtRu and $Pt_3Sn$ catalysts—A comparative DEMS study

H. Wang, Y. Zhao [1], Z. Jusys, R.J. Behm *

*Department Surface Chemistry and Catalysis, University of Ulm, D-89069 Ulm, Germany*

Available online 2 November 2005

**Abstract**

We present results of a comparative study on the interaction of ethylene glycol (EG) with carbon supported Pt, PtRu and $Pt_3Sn$ nanoparticle catalysts, employing electrochemical and quantitative differential electrochemical mass spectroscopy (DEMS) measurements under continuous reaction and continuous electrolyte flow conditions. For all three catalysts EG adsorption is inhibited at very cathodic adsorption potentials, dissociative adsorption starts above 0.06 V and increases with increasing potential. Based on the electron yield per formed $CO_2$ molecule and on the similarity with the $CO_{ad}$ stripping characteristics $CO_{ad}$ is identified as the main stable adsorbate; the relative coverage in terms of adsorbed C1 species, relative to that of a saturated CO adlayer on the respective catalyst, reaches a maximum of ca. 0.6 at around 0.4 V on Pt/Vulcan, ca. 0.2 at around 0.2 V on PtRu/Vulcan and ca. 0.4 at around 0.35 V on $Pt_3Sn$/Vulcan. Bulk EG electrooxidation under steady-state conditions shows a very small current efficiency for $CO_2$ formation of below 6% for 0.1 M EG on all three catalysts, the oxidation of EG mainly generates partly oxidized C2 by-products. Catalyst modification by Ru or Sn improves the activity for EG oxidation at low potentials ($\leq$0.56 V), but does not lead to better selectivities for complete EG oxidation to $CO_2$ at potentials with significant oxidation rates. Hence, C–C bond breaking is rate limiting for complete oxidation under present reaction conditions for all three catalysts. The data are consistent with a parallel pathway reaction mechanism, with formation and subsequent oxidation of $CO_{ad}$ in the one pathway and partial oxidation, via a sequence of reaction steps, to increasingly oxidized C2 species in the other pathway.


*Keywords:* Ethylene glycol oxidation; Supported catalyst; Pt/Vulcan; PtRu/Vulcan; $Pt_3Sn$/Vulcan; DEMS

## 1. Introduction

The electrochemical oxidation of ethylene glycol (EG) on platinum metal electrodes and catalysts has received significant attention during the last decades, both as a model compound for studies of the adsorption and electrooxidation behavior of C,O-containing organic species and due to its potential application as attractive anodic fuel in direct oxidation fuel cells (acidic solution [1–16], alkaline solution [3,5,8,17–22]). Previous studies have shown that, in addition to the complete oxidation product $CO_2$, EG electrooxidation leads to numerous partly oxidized, volatile by-products and stable adsorbates. The formation of adsorbed CO was observed by IR spectroscopy [3–5]. C2 partial oxidation products such as glycolaldehyde, glyoxal, glycolic acid, glyoxylic acid and oxalic acid, as well as C1 molecules (formaldehyde and formic acid) were identified via chromatography measurements during EG bulk electrooxidation, in addition to $CO_2$ production [2,8,10,13]. Based on these results a parallel reaction pathway with numerous intermediate steps was proposed, which involves the oxidation of the functional groups (–OH groups) without C–C bond rupture in the one pathway, and the splitting of the C–C bond with subsequent formation and oxidation of $CO_{ad}$ in the second pathway [13]. The influence of oxophyllic co-catalysts such as Ru and Sn on the EG oxidation performance was investigated by voltammetry [14–16] and in situ IR spectroscopy [15] as well as in fuel cell measurements [23,24].

Little is known, however, on the EG oxidation characteristics on a more quantitative scale and for reaction under reaction condition and on electrode materials being more closely related to fuel cell applications. We therefore started an extensive study on the oxidation of ethylene glycol and its oxidative derivatives under continuous reaction and continuous flow conditions on carbon supported Pt and bimetallic PtMe catalysts. Electrochemical and mass spectrometric (differential electrochemical

* Corresponding author.
*E-mail address:* juergen.behm@uni-ulm.de (R.J. Behm).
[1] Permanent address: Chemical Engineering College, Beijing Union University, Beijing 100023, PR China.

0378-7753/$ – see front matter © 2005 Elsevier B.V. All rights reserved.
doi:10.1016/j.jpowsour.2005.09.001

mass spectrometry—DEMS) measurements were applied in the present study to determine the Faradaic current and the selectivity for complete oxidation to $CO_2$ (current efficiency for $CO_2$ formation) under different reaction conditions and at different potentials. This study is closely related to a previous DEMS study on the kinetics and mechanism of ethanol adsorption and electrooxidation on carbon supported Pt and PtMe catalysts [25–27].

In the present paper we report results of a quantitative comparison between the EG adsorption and oxidation characteristics, including the EG oxidation activity and the selectivity for complete oxidation to $CO_2$, on commercial, carbon supported Pt, PtRu and $Pt_3Sn$ catalysts. Following a brief description of the experimental set-up and procedures we will first present and discuss results on EG adsorption on these catalysts in the potential range between the H-upd regime and the onset for EG bulk oxidation, applying chronoamperometric/chronocoulometric measurements of the adsorption transients at different constant potentials upon changing from inert base electrolyte to EG containing solution, and subsequent oxidative stripping of the adsorbed species. The second part of this section includes data on EG bulk oxidation over a range of potentials, via cyclovoltammetric and chronoamperometric measurements of the reaction transients at constant potential, after stepping the potential from 0.06 $V_{RHE}$ to the desired reaction potential, until steady-state conditions are reached. Applying proper calibration procedures the data allow us to quantitatively evaluate the selectivity for $CO_2$ formation for the different catalysts under fuel cell relevant reaction conditions (continuous reaction, controlled electrolyte transport). Finally, we will briefly discuss the implications of the present results on the use of EG as anodic feed in direct oxidation fuel cells (direct alcohol fuel cell—DAFC).

## 2. Experimental

The DEMS set-up and the preparation of the carbon (Vulcan XC-72) supported Pt and Pt alloy electrodes have been described in detail in previous publications [28–31]. In short, the DEMS set-up consists of two differentially pumped chambers, a Balzers QMS 112 quadrupole mass spectrometer, a Pine Instruments potentiostat and a computerized data acquisition system.

The thin-film Pt/Vulcan, PtRu/Vulcan and $Pt_3Sn$/Vulcan (20 wt.% metal loading, E-TEK Inc., mean particle size: $3.7 \pm 1.0$, $2.1 \pm 0.3$, $3.8 \pm 1.0$ nm; dispersion: 26, 44, and 27%, respectively) electrodes were prepared by pipetting and drying 20 μl of aqueous catalyst suspension (2 mg $ml^{-1}$) and then 20 μl Nafion aqueous solution on the central area of a mirror polished glassy carbon disk (Sigradur G from Hochtemperatur Werkstoffe GmbH, 9 mm in diameter), following procedures described earlier [28]. The catalyst thin film has a diameter of ca. 6 mm, resulting in a geometric surface area of 0.28 $cm^2$. Accordingly, the above procedure leads to a noble metal loading of 28 μg $cm^{-2}$. From the mean size of the nanoparticles the metal surface area of the Pt/Vulcan, PtRu/Vulcan and $Pt_3Sn$/Vulcan electrodes was calculated to be 6.1, 13.6 and 7.1 $cm^2$, respectively, assuming spherical particle shapes. From the H-upd desorption charge on Pt/Vulcan and from the (mass spectrometric) CO stripping charge we determined active surface areas of 5.9, 8.0 and 6.9 $cm^2$ for the Pt/Vulcan, PtRu/Vulcan and $Pt_3Sn$/Vulcan electrodes, respectively, which reflects the trends expected from the particle sizes. These data, the metal loadings, the geometric surface area or the active surface areas given above can be used also to convert the Faradaic currents given in all figures into mass specific currents or current densities, respectively.

The electrode was mounted into a dual thin-layer flow cell [32,33] and pressed against a 50 μm thick spacer. This leaves an exposed area of 0.28 $cm^2$ and results in an electrolyte volume of ~5 μl at the working electrode including connecting capillaries. The electrolyte flow was driven by the hydrostatic pressure in the supply bottle(s) (flow rate about 20–35 μl $s^{-1}$), ensuring a fast transport of the species formed at the working electrode to the mass spectrometric compartment, where the volatile products were evaporated into the mass spectrometer (time constant ca. 1 s) through a bare porous membrane (Scimat, 60 μm thick, 50% porosity, 0.2 μm pore diameter).

Two Pt wires at the inlet and outlet of the thin-layer cell, connected through an external resistance (1 MΩ), were used as counter electrodes. A saturated calomel electrode (SCE), connected to the outlet of the DEMS cell through the Teflon capillary, served as reference electrode. All potentials, however, are quoted against that of the reversible hydrogen electrode (RHE). The supporting electrolyte (0.5 M $H_2SO_4$) was prepared using Millipore Q water and ultrapure sulfuric acid (Merck, suprapur). Ethylene glycol (p.a.) was obtained from Merck, CO (N4.7) from Messer-Griesheim. Before the measurements all solutions were deaerated by high-purity Ar (MTI Gase, N6.0). All experiments were carried out at room temperature ($23 \pm 1$ °C).

For the chronoamperometric measurements of the current transients we connected two electrolyte supply bottles to the common inlet of the thin-layer flow cell, one with supporting electrolyte and the other one with a solution containing 0.1 M ethylene glycol to ensure a constant mass transport to the electrode during adsorption. The Faradaic current transients on the clean catalysts were measured for 5 min at constant electrode potential, after switching from pure supporting electrolyte to ethylene glycol containing solution. After passing ethylene glycol solution through the flow cell for 5 min at the respective reaction potential, the potential was stepped to 0.06 V, where the adsorbed ethylene glycol decomposition products cannot be desorbed (this was tested in additional DEMS measurements) and further adsorption is inhibited (see below). The remaining ethylene glycol in the solution was removed by exchanging the solution with pure 0.5 M $H_2SO_4$ solution and extensive rinsing (ca. 3 min) with that electrolyte. Subsequently, the potential was scanned positively to oxidize the adsorbed species. Both the electrochemical signal and $CO_2$ formation (mass spectrometric signal at $m/z = 44$) were followed. The relative amount or coverage of adsorbed C1 species ($CO_{ad}$) compared to that of a saturated CO adlayer on the respective catalyst was quantified by comparison with the amount of $CO_2$ formed after oxidation of a saturated CO adlayer produced upon adsorption from a CO saturated electrolyte. The average number of electrons per $CO_2$ molecule formed during electrooxidation of the adsorbed

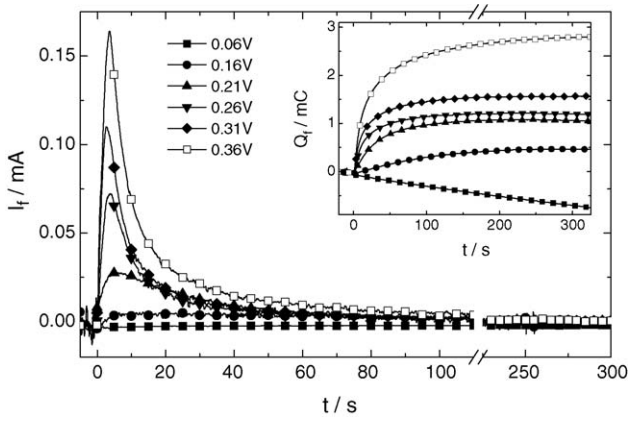


Fig. 1. Chronoamperometric and the corresponding chronocoulometric (inset) transients for the adsorption of ethylene glycol on a Pt/Vulcan catalyst electrode at different, constant electrode potentials (potentials see figure). For adsorption, the electrolyte was switched at $t = 0$ from the supporting electrolyte (0.5 M $H_2SO_4$ solution) to a solution containing 0.1 M ethylene glycol.

species was calculated as $n = K^* Q_f/Q_i$, where $Q_f$ and $Q_i$ are the Faradaic charge and corresponding mass spectrometric charge during the oxidation of the adsorbate. $K^*$ denotes the calibration constant of the DEMS set-up, which was determined by calibration measurements using the oxidation of a preadsorbed (from CO saturated electrolyte) CO adlayer ('CO stripping') for EG adsorbate stripping [31] or CO bulk oxidation for EG bulk oxidation. The resulting $K^*$ values differ slightly because of the different contributions from pseudocapacitive charging [34]. The current efficiencies for $CO_2$ formation from EG were calculated assuming the formal value of five electrons per carbon atom (or per $CO_2$ molecule formed). This value was also used to calculate the current contribution from $CO_2$ formation, which does not include possible effects arising from the fact that $CO_2$ formation from $CO_{ad}$ and $CO_{ad}$ formation from EG decomposition may take place at different potentials. Because of the very low current efficiencies for $CO_2$ formation the errors introduced by this assumption are small, at least on an absolute scale.

## 3. Results and discussion

### 3.1. Dissociative adsorption of ethylene glycol

In these experiments we followed the evolution of the Faradaic current and of the mass spectrometric $CO_2$ ion signal with time at different constant adsorption potentials up to the onset of EG bulk oxidation, after switching from pure supporting electrolyte to 0.1 M EG containing solution.

#### 3.1.1. Ethylene glycol adsorption on carbon supported Pt

The current response of a Pt/Vulcan catalyst upon interaction with EG solution in the initial adsorption period (300 s) and for different adsorption potentials between 0.06 and 0.36 V is displayed in Fig. 1. The related integrated coulometric charges (chronocoulometric transients) over the entire adsorption time of 5 min are shown in the inset. At 0.06 V EG adsorption is nearly completely inhibited, which is supported also by the negligible charge in the subsequent stripping signal (see Fig. 3). In fact, negative currents are obtained at 0.06 V due to the onset of $H_2$ evolution. The inhibition of EG adsorption is explained by surface blocking due to H-upd, which closely resembles previous observations for ethanol adsorption on the same catalyst [25]. Going to higher potentials ($\leq$0.36 V), we find increasing anodic currents (charges) upon EG adsorption. The current signal rises steeply upon admission of the electrolyte, passes through a maximum and then decays in a roughly exponential way. The anodic peak current increases progressively when going to more positive adsorption potentials. Likewise, the initial increase of the adsorption charge with time becomes steeper, and the saturation adsorption charge increases for more positive adsorption potentials. At potentials >0.36 V, the oxidative charge always increases with time, due to the bulk oxidation of EG (see Section 3.2).

The total amount of adsorbed decomposition products formed upon adsorption (ca. 5 min adsorption time) is determined by oxidation in a subsequent potential scan to 1.16 V ('EG adsorbate stripping'), after having changed to pure supporting electrolyte. It should be noted that we did not see any evolution of methane or ethane after stepping the potential from the adsorption potential to 0.06 V in these experiments (electrolyte exchange prior to the CV), which rules out contributions from reductive adsorbate stripping, in contrast to ethanol adsorbate [25]. The Faradaic current signals and the mass spectrometric currents for $CO_2$ ($m/z = 44$) resulting from ethylene glycol adsorbate stripping are shown in Fig. 2. The almost complete absence of the H-upd desorption signal indicates that the surface is largely covered by adsorbed decomposition products. The shape and potential (ca. 0.65 V) of the subsequent anodic peak closely resembles that for the oxidation of adsorbed CO resulting from decomposition of other alcohols such as methanol or ethanol [25,30], suggesting already that EG adsorption results in adsorbed CO as the main stable adsorbate. This preliminary assignment will be substantiated by the calculated number of electrons generated per $CO_2$ product molecule as discussed below, and fully agrees with results of previous IR measurements [10,11]. The current behavior at higher potentials is identical to that of the base CV (second scan in the same electrolyte, see Fig. 2a, dotted line). The $CO_2$ ion current signal closely follows the Faradaic current peak. From the absence of any $CO_2$ formation and from the characteristic H-upd features in the negative-going scan and also in the second positive-going scan we conclude that all decomposition products were oxidized in the first positive-going stripping scan.

The total amount of oxidizable, stable adsorbates formed upon EG admission was determined from the mass spectrometric $CO_2$ signal (Fig. 2b), since the oxidative charge in the Faradaic current peak includes contributions from double-layer charging as well, which result, e.g. from the shift of the potential of zero charge and ion readsorption [25,33]. This way we obtained a relative coverage of about $\theta_{max} = 0.58\ \theta_{CO,sat}$ at ca. 0.4 V, relative to that of a saturated CO adlayer on that catalyst ($\theta_{CO,sat}$), assuming that all adsorbed species contain one carbon atom each. Going to lower adsorption potentials we find similar

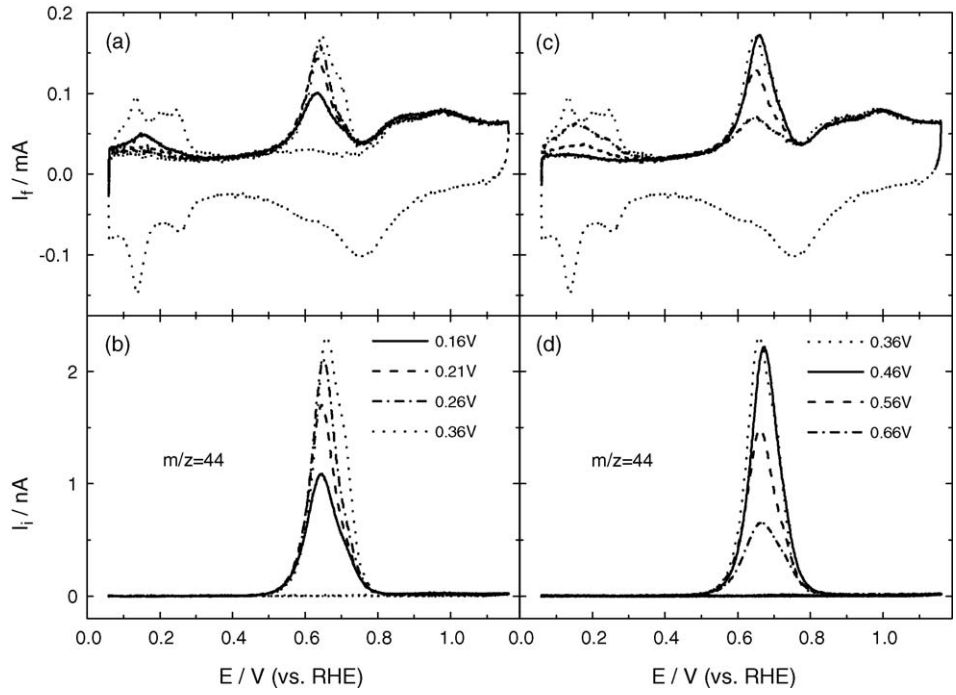


Fig. 2. Simultaneously recorded CVs (a, c) and MSCVs of $m/z = 44$ (b, d) for the oxidation of ethylene glycol adsorbate formed upon adsorption on a Pt/Vulcan catalyst electrode at increasing potentials (scan rate: 10 mV $s^{-1}$). The adsorption potentials are given in the figure. Dotted line: first negative-going scan and second positive-going scan (base CV/MSCV).

stripping characteristics, but lower adsorbate coverages. Hence, under these conditions EG adsorption is less efficient. Finally, the adsorbate coverage approaches zero for 0.06 V adsorption potential, reflecting the increasing site blocking by $H_{upd}$ (see Fig. 3). The decay in adsorbate coverage at higher adsorption potentials is attributed to the onset of adsorbate oxidation.

The number of electrons generated per $CO_2$ molecule formed by oxidation of the decomposition products upon EG adsorption is listed for different adsorption potentials in Table 1. It shows that the calculated number of electrons per $CO_2$ molecule is larger than 2 at 0.16 V, decreases with increasing potential to values close to 2 around 0.4 V, and then increases again.

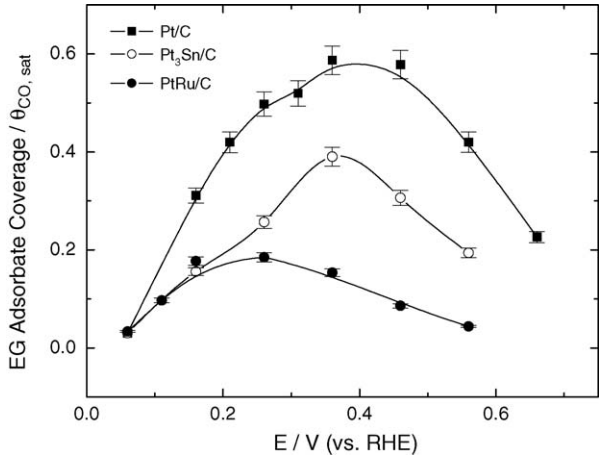


Fig. 3. Relative coverages of ethylene glycol adsorbate compared to that of a saturated CO adlayer obtained at different adsorption potentials on the Pt/Vulcan, PtRu/Vulcan and $Pt_3Sn$/Vulcan catalyst electrode.

These results support the above conclusion that $CO_{ad}$ is the dominant, stable adsorbate, at least for adsorption potentials around 0.4 V. The higher number of electrons per $CO_2$ obtained at lower potentials is tentatively attributed to relatively larger capacitive charge contributions at low $CO_{ad}$ coverages under these conditions rather than to other, non-$CO_{ad}$ species on the catalyst surface, since IR results indicate that only $CO_{ad}$ are being present [10,11].

### 3.1.2. Ethylene glycol adsorption on carbon supported PtRu

Similar current transients as shown above for ethylene glycol adsorption on Pt/Vulcan are presented in Fig. 4 for EG adsorption on PtRu/Vulcan at different adsorption potentials between 0.06 and 0.36 V. The related integrated coulometric charges (chronocoulometric transients) are displayed in the inset. Similarly to

Table 1
Number of electrons generated per $CO_2$ molecule formed during the electrooxidation of EG decomposition products resulting upon ethylene glycol adsorption on Pt/Vulcan

| $E$ (V) | $n$ (Pt) |
|---|---|
| 0.16 | 2.6 |
| 0.21 | 2.4 |
| 0.26 | 2.3 |
| 0.31 | 2.4 |
| 0.56 | 2.2 |
| 0.46 | 2.2 |
| 0.56 | 2.4 |
| 0.66 | 2.5 |

$E$: adsorption potential; $n$: electron number.

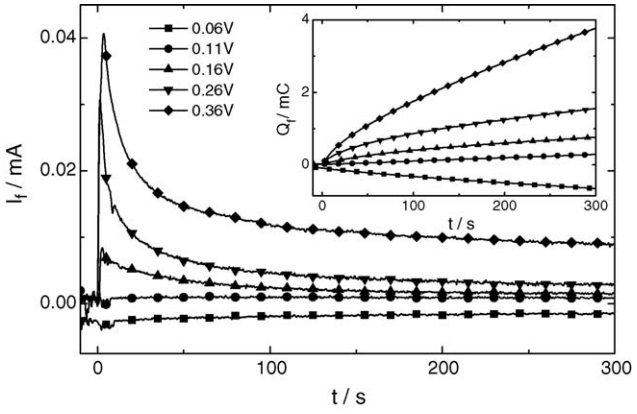


Fig. 4. Chronoamperometric and the corresponding chronocoulometric (inset) transients for the adsorption of ethylene glycol on a PtRu/Vulcan catalyst electrode at different, constant electrode potentials (potentials see figure). For adsorption, the electrolyte was switched at $t = 0$ from the supporting electrolyte (0.5 M $H_2SO_4$ solution) to a solution containing 0.1 M ethylene glycol.

the adsorption behavior on Pt/Vulcan EG adsorption is practically inhibited at the most cathodic potential (0.06 V), which is supported also by the very small adsorbate coverage determined from adsorbate stripping in Figs. 3 and 5. The anodic currents (charges) upon EG adsorption increase with increasing potentials. Compared to Pt/Vulcan, the maximum anodic current is markedly reduced, indicating that the presence of Ru surface atoms tends to inhibit the dissociative adsorption of ethylene glycol. This tendency agrees well with earlier reports for room temperature methanol adsorption [35] and ethanol adsorption [27]. At potentials of ≥0.3 V EG bulk oxidation sets in (see also Fig. 11), which is responsible for the continuously increasing integrated anodic charge.

The total amount of adsorbed EG decomposition products formed upon adsorption is again determined by oxidative stripping, after having changed to pure supporting electrolyte. In order to avoid dissolution of Ru, these scans were limited to a maximum potential of 0.76 V. Since this may not be sufficient to completely oxidize the adsorbed species, three more cycles were added. Also for the PtRu/Vulcan catalyst reductive formation of methane or ethane can be ruled out. The Faradaic current signals and the mass spectrometric currents of $CO_2$ ($m/z = 44$) for EG adsorbate stripping are shown in Fig. 5. The total amount of oxidizable, stable adsorbates formed upon EG admission was determined from the mass spectrometric $CO_2$ signal (Fig. 5b).

Fig. 5b illustrates that the oxidation of EG adsorbate starts at ca. 0.3 V, which is shifted negatively by over 100 mV compared to that on Pt/Vulcan, and the main oxidative peak is also shifted negatively, by over 50 mV. It is well known that on PtRu and PtRu/Vulcan catalysts $CO_{ad}$ oxidation is enhanced compared to Pt [36–43], which agrees well with our present findings. The relative coverages of EG adsorbate on PtRu/Vulcan, calculated as described above, are shown again in Fig. 3. Similarly as on Pt/Vulcan, the coverage of EG adsorbate increases with increasing potential, reaches a maximum (ca. 0.2 $\theta_{CO,sat}$) around 0.2 V, and then decreases due to the oxidation of EG adsorbate at potentials positive of 0.26 V. Compared to Pt/Vulcan, the coverage of EG adsorbate is much smaller on PtRu/Vulcan. This equally

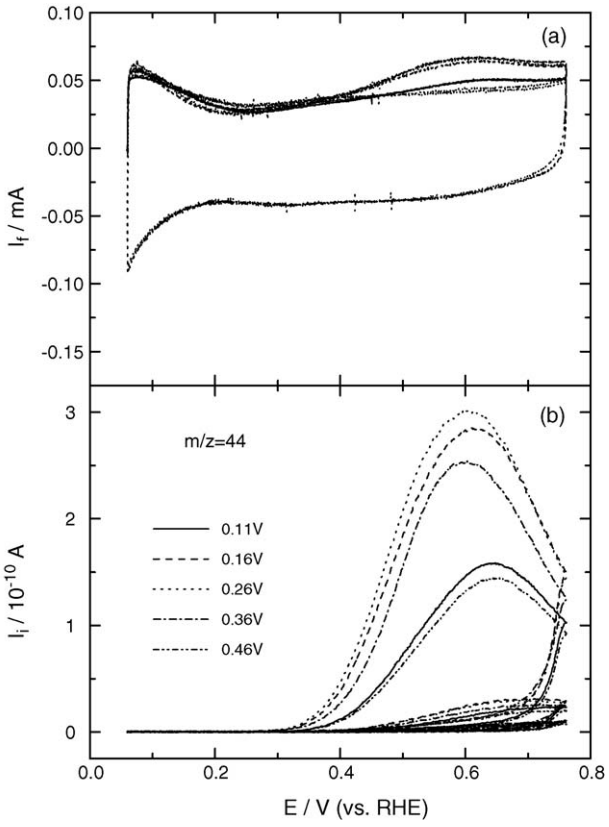


Fig. 5. Simultaneously recorded CV (a) and MSCV of $m/z = 44$ (b) for the oxidation of ethylene glycol adsorbate formed upon adsorption on a PtRu/Vulcan catalyst electrode at different potentials (scan rate: 10 mV $s^{-1}$). The adsorption potentials are given in the figure.

indicates that PtRu/Vulcan is not favorable for EG dissociative adsorption at ambient temperatures compared to Pt/Vulcan.

### 3.1.3. Ethylene glycol adsorption on carbon supported $Pt_3Sn$

The current transients for ethylene glycol adsorption on $Pt_3Sn$/Vulcan at different adsorption potentials between 0.06 and 0.36 V are shown in Fig. 6. The related integrated coulometric charges (chronocoulometric transients) are displayed in the inset. Again, at 0.06 V EG adsorption is practically inhibited (very small coverage of EG adsorbate, see Fig. 3), and the anodic currents (charges) upon EG adsorption increase with increasing potential. Compared to Pt/Vulcan, the maximum anodic current is markedly reduced. This indicates that the presence of Sn reduces the activity for dissociative adsorption of EG, which is equivalent to lowering the activity for C–C bond breaking. Sn alloying with Pt decreases the number of surface Pt ensembles compared to Pt/Vulcan, which are considered as active sites for C–H bond breaking [44]. At potentials positive of 0.26 V (e.g., 0.36 V) EG bulk oxidation sets in (Fig. 13), therefore the integrated oxidative charge is not only associated with the decomposition adsorption, but also with EG bulk oxidation.

The total amount of adsorbed decomposition products formed upon adsorption is again determined by oxidation in a subsequent potential scan to 0.96 V ('adsorbate stripping'), after having changed to pure supporting electrolyte. (Because of the

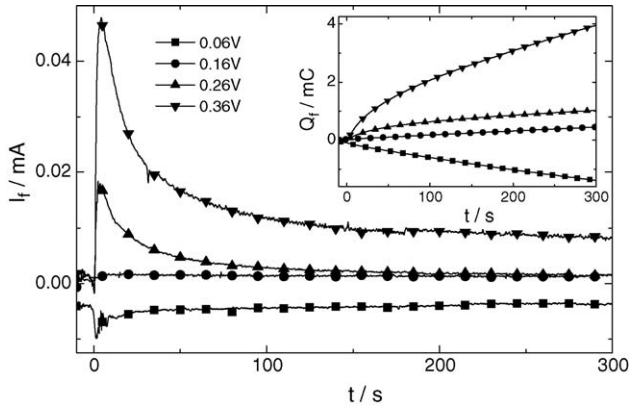


Fig. 6. Chronoamperometric and the corresponding chronocoulometric (inset) transients for the adsorption of ethylene glycol on a $Pt_3Sn$/Vulcan catalyst electrode at different, constant electrode potentials (potentials see figure). For adsorption, the electrolyte was switched at $t = 0$ from the supporting electrolyte (0.5 M $H_2SO_4$ solution) to a solution containing 0.1 M ethylene glycol.

high positive potential limit in these scans and the danger of Sn dissolution each adsorption/stripping experiments was done with a new catalyst electrode.) The Faradaic current signals and the mass spectrometric currents of $CO_2$ ($m/z = 44$) for EG adsorbate stripping are shown in Fig. 7. The total amount of oxidizable, stable adsorbates formed upon EG admission was

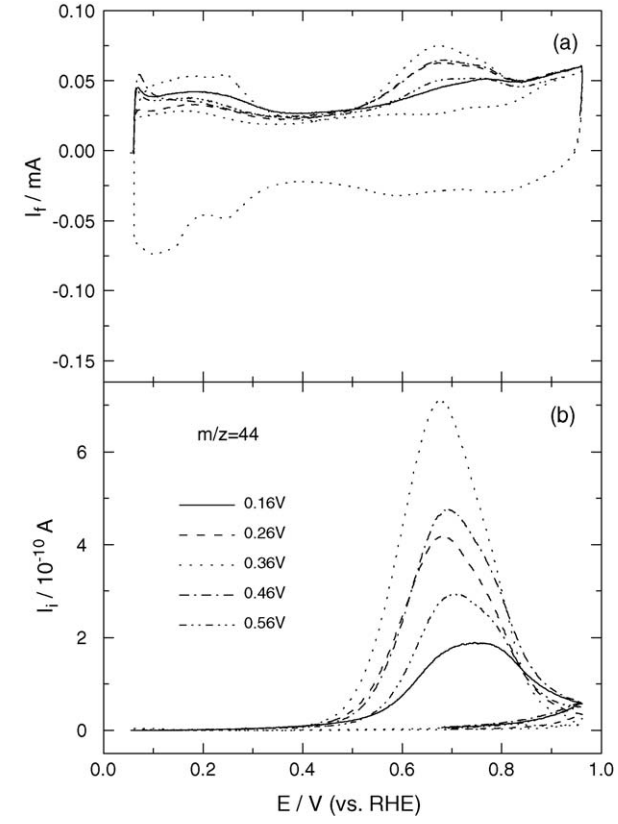


Fig. 7. Simultaneously recorded CV (a) and MSCV of $m/z = 44$ (b) for the oxidation of ethylene glycol adsorbate formed upon adsorption on a $Pt_3Sn$/Vulcan catalyst electrode at different potentials (scan rate: l0 mV $s^{-1}$). The adsorption potentials are given in the figure. Dotted line: first negative-going scan and second positive-going scan (base CV/MSCV).

determined from the mass spectrometric $CO_2$ signal (Fig. 7b). The oxidation of EG adsorbate starts from ca. 0.2 V, shifted negatively by over 200 mV compared to Pt/Vulcan. A similar behavior is well known for $CO_{ad}$ oxidation and has been explained by a 'bifunctional mechanism', with CO adsorption on Pt sites and facile $OH_{ad}$ formation on Sn sites [38]. However, only small amounts of EG adsorbate are oxidized in the low potential region ($\leq$0.45 V), the main $CO_2$ formation signal starts at about 0.4 V and has its maximum at about 0.67 V, which is close to the respective potentials observed on Pt/Vulcan. The relative coverages of EG adsorbate, calculated as described above, are shown in Fig. 3. Similarly as on Pt/Vulcan, the relative coverage of EG adsorbate increases with increasing potential, reaches its maximum (ca. 0.4 $\theta_{CO,sat}$) for adsorption at 0.36 V, and then decreases again due to the onset of EG adsorbate oxidation at potentials positive of 0.36 V. Compared to Pt/Vulcan, the (relative) coverage of EG adsorbate is significantly smaller on $Pt_3Sn$/Vulcan. Since the relative coverages are normalized to the $CO_{ad}$ saturation coverage on the $Pt_3Sn$ catalyst, the decrease of the maximum EG adsorbate coverage compared to Pt/Vulcan significantly exceeds the effect caused by the reduction in Pt sites on the bimetallic catalyst, indicating that the deactivation for EG decomposition exceeds the effects caused by site blocking (replacement of Pt surface atoms by Sn).

### 3.2. Bulk oxidation of ethylene glycol

In this section we compare ethylene glycol bulk oxidation on the three different carbon supported PtX catalysts by potentiodynamic measurements and by potentiostatic, chronoamperometric measurements. The latter measurements, which allow us to distinguish between time and potential effects, were performed by stepping the potential from initially 0.06 V to the respective reaction potential between 0.36 and 0.76 V. In addition to Faradaic current measurements we followed the reaction by monitoring the $CO_2$ ($m/z = 44$) ion current. No other mass signals were detected during EG oxidation in these measurements.

#### 3.2.1. Ethylene glycol oxidation on carbon supported Pt

The cyclic voltammogram (CV) and the corresponding mass spectrometric cyclic voltammogram (MSCV) for EG oxidation on a carbon supported Pt catalyst electrode are reproduced in Fig. 8a and b. CVs with similar characteristics were reported in previous studies (see references in Section 1), but much of the information results from the comparison with the $CO_2$ signal, as will be shown below. The CV (Fig. 8a, solid line) starts with a weak anodic current in the low potential region (<0.4 V) in the first positive-going scan, but no corresponding $CO_2$ formation (Fig. 8b, solid line). Therefore, this must be associated with dissociative EG adsorption or/and bulk oxidation to other reaction intermediates. The onset of EG oxidation (Faradaic current) occurs at about 0.35 V in this scan, leading to an asymmetric peak with a maximum at 0.68 V and significant intensity in the high potential side (Fig. 8a, solid line). At the most positive potentials ($E > 1.0$ V) the oxidation current starts to increase again. $CO_2$ formation starts only at higher potential than the

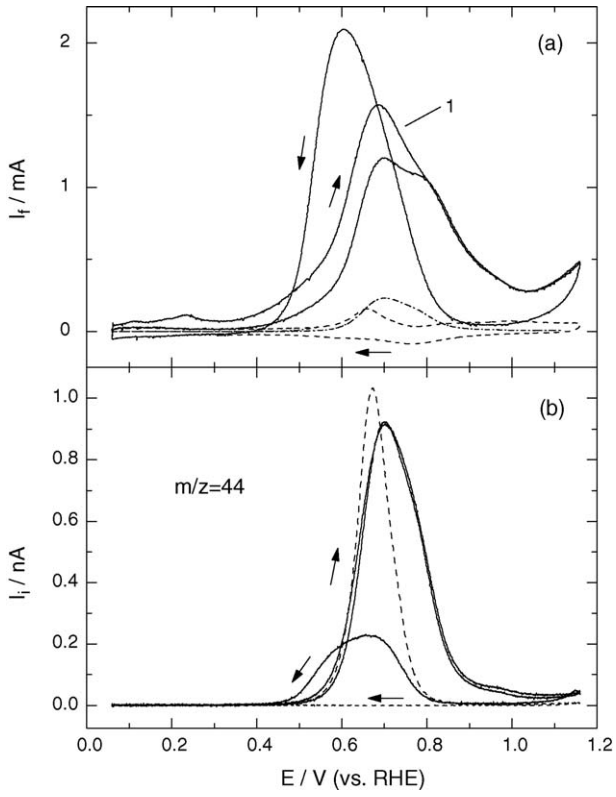


Fig. 8. Simultaneously recorded CVs (a) and $m/z$ =44 MSCVs (b) on a Pt/Vulcan catalyst electrode in 0.1 M ethylene glycol + 0.5 M $H_2SO_4$ solution (full lines); dashed line: oxidative stripping of the ethylene glycol adsorbate formed at 0.46 V (full cycle). The calculated contribution of $CO_2$ formation to the Faradaic current signal is indicated by the dash-dotted line (scan rate: 10 mV $s^{-1}$).

Faradaic current, at around 0.5 V. Furthermore, the subsequent peak is much more symmetric than the Faradaic current peak, with a main maximum at 0.70 V and little additional intensity if any in the high potential side (Fig. 8b, solid line). Hence, the qualitative comparison indicates already that only the main oxidation peak may be due to $CO_2$ formation (see below for quantitative evaluation), while the high potential shoulder and the current increase at >1.0 V must result from the formation of reaction intermediates or by-products. In the second and subsequent positive-going scans the current signal in the low potential region (<0.4 V) has disappeared. The onset of the main oxidation peak is again at about 0.35 V, but now it leads to a clearly resolved double peak structure with a main peak at 0.7 V and a shoulder at 0.79 V (Fig. 8a, solid line). Compared to the first positive-going scan the intensity in the low potential peak is much lower in the second positive-going scan. The $CO_2$ ion current, in contrast, has hardly changed from the first to the second positive-going scan, indicating that the reduced signal in the second positive-going scan is only caused by a reduction in the formation of partly oxidized C2 by-products (Fig. 8b, solid line). In the negative-going scan, we find an asymmetric anodic current peak, which starts at 0.9 V, then increases steadily to a maximum at 0.6 V and finally drops steeply to zero (Fig. 8a). The related $CO_2$ ion current signal (Fig. 8b, solid line) is much weaker than in the positive-going scan, in contrast to the higher current in the Faradaic current signal. Hence, the tendency for $CO_2$ formation is much weaker in the negative-going scan than in the positive-going scan. Furthermore, the $CO_2$ signal resolves two components, centered at 0.7 and 0.6 V, respectively (Fig. 8b). In the Faradaic current signal the low potential component is dominant, while it is slightly weaker than the high potential component in the $CO_2$ signal.

The contribution of $CO_2$ formation to the Faradaic current signal, which is calculated from the $m/z$ = 44 signal (see dash-dotted line in Fig. 8a), is on the order of a few percent during the scan. The agreement in the shape and potential of the main Faradaic current peak and that for $CO_2$ formation therefore indicate that, although the latter process contributes only little to the Faradaic current, the dominant reaction pathway must be governed by the same surface conditions/reaction steps as that for $CO_2$ formation. Also, we can practically rule out the possibility that the $CO_2$ signal contains contributions from the fragmentation of other volatile by-products. (Note that most of the potential by-products are not sufficiently volatile to be detected by standard DEMS, but readily desorb from the catalyst surface.) These should also result in other fragments, and we did not resolve potential dependent features in other masses. For the high potential shoulder and the current increase at >1.0 V, where $CO_2$ formation is absent, the situation is different. Since $CO_{ad}$ oxidation would be facile in this potential range, we conclude that C–C bond breaking is practically inhibited at potentials >0.7 V on Pt/Vulcan. The average current efficiency for $CO_2$ formation, integrating over a complete cycle is only ca. 6%, with 9.5% in the positive-going scan and 2.6% in the negative-going scan (see Table 2), i.e., for reaction at ambient temperatures EG oxidation on carbon supported Pt produces mainly C2 reaction intermediates and by-products, without C–C bond breaking.

Comparing EG bulk oxidation with EG adsorbate oxidation (dashed 1ine in Fig. 8 for EG adsorbate stripping after adsorption at 0.46 V), we see that although the bulk oxidation current starts already at lower potential and is much larger than that of EG adsorbate oxidation, the onset potentials for $CO_2$ formation are same for EG bulk oxidation and EG adsorbate oxidation. Furthermore, the $CO_2$ ion currents are also nearly the same in the lower oxidation potential range. Only at higher potentials we find more $CO_2$ intensity for EG bulk oxidation, resulting in a wider $CO_2$ formation for EG bulk oxidation than for EG adsorbate stripping. The total amount of $CO_2$ formed in the two cases, is though not exactly identical, of similar magnitude. This seems to suggest that $CO_2$ is largely formed via oxidation of $CO_{ad}$ formed during EG oxidation in the lower potential range. The

Table 2
The average current efficiency for $CO_2$ formation ($A_q(CO_2)$) in a full cyclic scan in 0.1 M ethylene glycol on different electrodes (polycrystalline Pt see Ref. [51])

| Electrode | $A_q(CO_2)$ (%) |
|---|---|
| pc-Pt[a] | 3.9 |
| pc-Pt[b] | 6.2 |
| Pt/Vulcan[a] | 5.5 |
| PtRu/Vulcan | 6.7 |
| $Pt_3Sn$/Vulcan | 4.0 |

[a] Upper potential limit 1.16 V.
[b] Upper potential limit 1.51 V.

main EG oxidation current, however, results from partial EG oxidation to different C2 molecules. This mechanistic finding of at least two reaction pathways, one leading to $CO_2$ via formation and oxidation of $CO_{ad}$ and the other one resulting in incomplete oxidation products maintaining the C–C bond, resembles earlier predictions based on electrochemical and in situ IR spectroscopic measurements [10], but so far the current efficiency for $CO_2$ formation had not been quantified, and also the pronounced differences in $CO_2$ formation between positive-going and negative-going scan had not be reported so far. It should be noted that the incomplete oxidation by-products can be further oxidized via subsequent readsorption, after desorption, and continuing reaction. The tendency for this is more pronounced on high surface area electrodes and catalysts [45,46].

Finally we would like to note that similar measurements performed on a smooth polycrystalline Pt electrode showed an even lower current efficiency for $CO_2$ formation than on Pt/Vulcan. We explain this difference by readsorption effects, which contribute differently for the two electrodes due to their different roughness or specific surface areas. The Pt/Vulcan electrode has a roughness factor of 20, while for smooth polycrystalline Pt the roughness factor is below 2. In the case of Pt/Vulcan, partially oxidized reaction intermediates or by-products have a higher chance to readsorb again, after desorption from the Pt surface, and undergo further oxidation before they leave the surface near region and diffuse into the solution. For the smooth Pt electrode readsorption is much less probable. Such effects had been investigated in detail and demonstrated for methanol oxidation on Pt/Vulcan catalysts, evaluating the product distribution for different catalyst loadings and, for comparison, for a smooth polycrystalline Pt electrode [45,46].

More information on the steady-state situation during EG oxidation and on the effect of the reaction potential is obtained from potential-step experiments, performed for reaction potentials between 0.46 and 0.81 V. Selected Faradaic current and the corresponding ion current ($m/z = 44$) transients for ethylene glycol oxidation on Pt/Vulcan at different potentials are shown in Fig. 9. Prior to the potential step transient the potential is first stepped to 1.16 V for 3 s to clean the surface, then back to 0.06 V. At the initial potential (0.06 V) the catalyst surface should be free of EG adsorbate. The pronounced current spike of the Faradaic current transients can be attributed to contributions from double-layer charging. Comparison with the $CO_2$ ion current transients, which equally exhibit an initial current spike, reveals that this spike also includes contributions from an initial maximum in the reactivity, which must be related to the change in the adsorbate layer and, at higher reaction potentials, also of the Pt surface. A possible mechanism involves rapid $CO_{ad}$ formation during the potential jump and reaction with $OH_{ad}$ surface species equally formed during that process. At longer reaction times the surface develops its steady-state adlayer coverage, which leads to a partial blocking of the surface.

After passing through the initial spike the Faradaic current decreases only little with time and has quickly reached a quasi-steady-state value. For the $CO_2$ ion current the spike is much less pronounced compared to the subsequent steady-state signal. Its increase with higher reaction potential can be explained by the

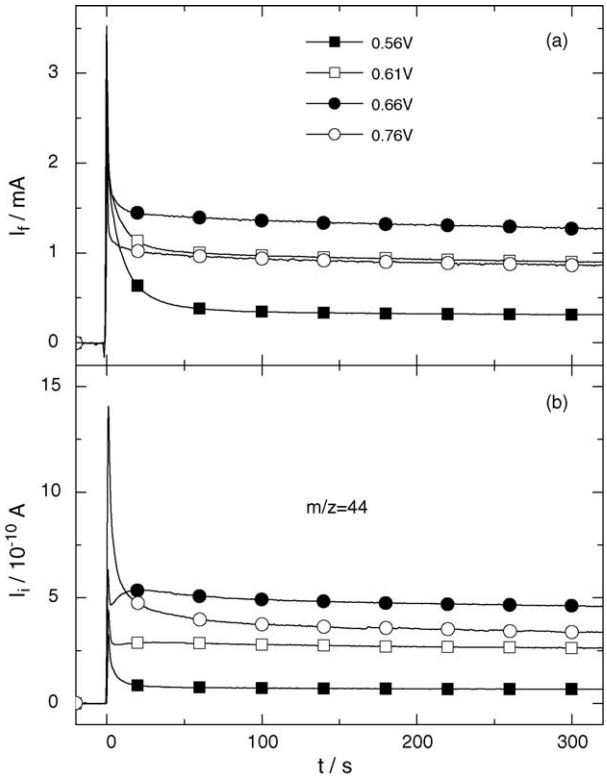


Fig. 9. Faradic current (a) and the corresponding $m/z = 44$ ion current transients (b) after a potential step from 0.06 V to different reaction potentials (reaction potentials see figure) on a Pt/Vulcan catalyst electrode in 0.1 M ethylene glycol + 0.5 M $H_2SO_4$ soluti on.

increasing amount of instantaneously formed oxygen containing species. For low and high reaction potentials the $m/z = 44$ ion current changes with time are analogous to those of the Faradaic current. For medium reaction potentials, however, the $CO_2$ ion current increases with time after the steep decay from the initial spike, passing through a weak maximum after several seconds. Subsequently the signal decays slightly and also reaches its steady-state value during the following minutes. Apparently, this weak maximum in the $CO_2$ formation rate is masked by other dominant contributions to the Faradaic current in the latter signal. The weak maximum in the $CO_2$ formation rate can be tentatively explained by a reaction scheme where $CO_2$ formation is limited by the formation of oxygen containing species at low potentials and by C–C bond breaking/$CO_{ad}$ formation at high potentials, and both of these rapidly assume their steady-state rates. At medium reaction potentials the $CO_2$ formation rate depends on both rates and on the respective coverages, which can lead to more complex time dependences.

The Faradaic currents and the corresponding current efficiencies for $CO_2$ formation under steady-state conditions, after 5 min reaction, are plotted for the different reaction potentials in Fig. 10. The Faradaic current (Fig. 10a) and the corresponding current efficiency for $CO_2$ formation (Fig. 10c) increase steadily from the lowest reaction potential (0.46 V), although the variations in the $CO_2$ current efficiency are rather small, between 3 and 5%. The Faradaic current reaches a maximum at 0.67 V and then decays again; the $CO_2$ current efficiency assumes its maxi-

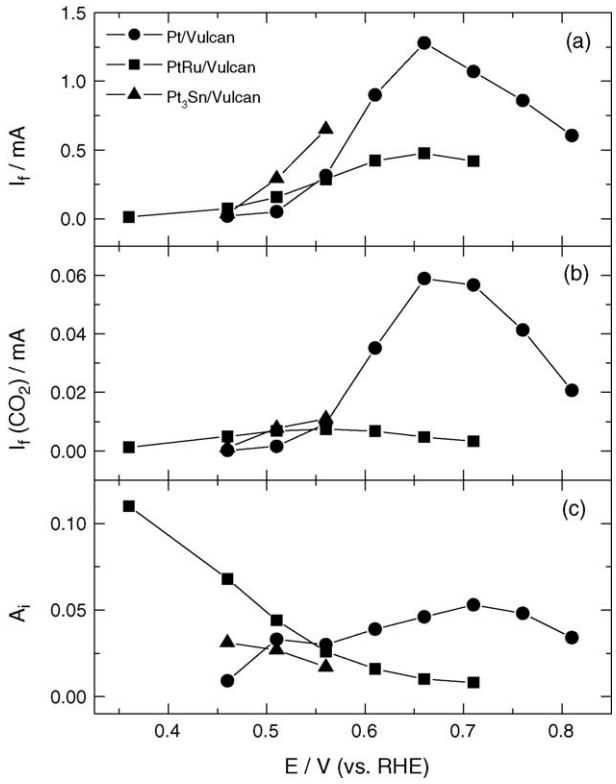


Fig. 10. Steady-state total Faradaic currents (a), steady-state Faradaic currents for $CO_2$ formation (b) and current efficiencies for $CO_2$ formation (c) as a function of the reaction potential for the different carbon supported PtX catalyst electrodes (catalyst see figure).

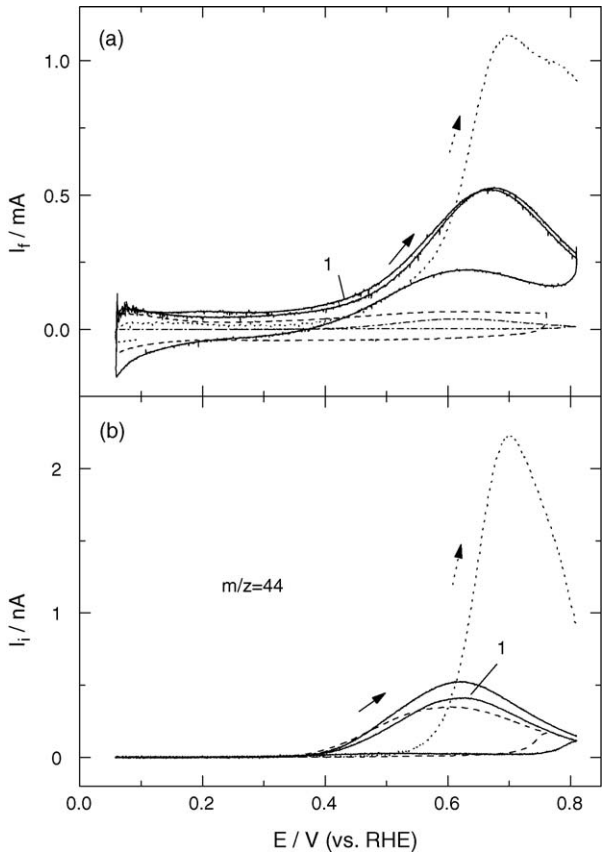


Fig. 11. Simultaneously recorded CVs (a) and $m/z = 44$ MSCVs (b) on a PtRu/Vulcan catalyst electrode in 0.1 M ethylene glycol + 0.5 M $H_2SO_4$ solution (full lines); dashed line: oxidative stripping of the ethylene glycol adsorbate formed at 0.26 V (full cycle). For comparison, the signals for ethylene glycol bulk oxidation on a Pt/Vulcan catalyst electrode are also shown (dotted line). The calculated contribution of $CO_2$ formation to the Faradaic current signal (a) is indicated by the dash-dotted line (scan rate: 10 mV $s^{-1}$).

mum of slightly above 5% at 0.71 V and then it drops again with higher reaction potential. Also under potentiostatic, steady-state conditions ethylene glycol oxidation largely results in incomplete oxidation by-products (C2 species), complete oxidation to $CO_2$ is only a minority pathway under present reaction conditions. The low probability for $CO_2$ formation is attributed to the kinetic barrier for C–C bond breaking under current reaction conditions. Similar observations were reported recently for ethanol oxidation on carbon supported Pt catalysts and polycrystalline Pt electrodes [26], confirming the above interpretation.

### 3.2.2. *Ethylene glycol oxidation on PtRu/Vulcan*

The activity of carbon supported PtRu catalysts for EG oxidation and their selectivity for complete oxidation to $CO_2$ was equally evaluated by cyclic voltammetry and by potential-step oxidation transients. Cyclic voltammograms (CV, first cycle plus second positive-going scan) and the corresponding mass spectrometric cyclic voltammograms (MSCV) recorded in EG containing solution on a PtRu/Vulcan catalyst electrode are shown in Fig. 11 (solid lines). For comparison, we also include the CVs and MSCVs of EG adsorbate stripping on PtRu/Vulcan (Fig. 11a, dashed line, after EG adsorption at 260 mV, full cycle, from Fig. 5) and EG bulk oxidation on the Pt/Vulcan catalyst (Fig. 11, dotted line, from Fig. 8) as well as the Faradaic current contribution from $CO_2$ formation (dash-dotted line, Fig. 11a). In order to avoid Ru dissolution the upper limit of the potential scan was set to 0.81 V.

On the PtRu/Vulcan catalyst electrode EG oxidation starts around 0.3 V, which is 50 mV more negative than on Pt/Vulcan. $CO_2$ formation starts again only at more positive potentials, the onset potential is around 0.35 V (Fig. 11b, solid line). While this is more positive compared to the Faradaic current signal, it is about 150 mV more negative than the onset for $CO_2$ formation on the Pt/Vulcan electrode under similar conditions, i.e., the presence of Ru can enhance both the formation of partly oxidized reaction intermediates as well as that of $CO_2$ formation. After passing through a maximum at 0.68 V the oxidation current decreases again. The potential of the maximum current on PtRu/Vulcan (Fig. 11a, solid line) almost coincides with that on Pt/Vulcan (Fig. 8a, solid line). For identical catalyst loading the current is, however, significantly less than on the latter catalyst electrode, around 0.5 mA as compared to about 1.1 mA on Pt/Vulcan. The loss in activity at the highest potential is attributed to the oxidation of Ru, e.g., from hydrous Ru oxide into an inactive oxide state [47]. The $CO_2$ ion current signal peaks at 0.61 V and decays to almost zero at the upper potential limit of 0.8 V (Fig. 11b, solid line). Hence, also in this case $CO_2$ formation occurs mainly in the first part of the broad Faradaic current peak. The contribution from $CO_2$ formation to the Faradaic cur-

rent, which is indicated by the dash-dotted line in Fig. 11a, is again very low. Similar to the situation for EG oxidation on Pt/Vulcan, $CO_2$ formation must be dominated by the same catalyst surface conditions as the total Faradaic current to explain the similar reaction onset and peak potential. Different from the Pt/Vulcan catalyst electrode, however, we observe very little $CO_2$ formation in the reverse scan, i.e., C–C bond breaking and $CO_{ad}$ formation are almost completely inhibited at higher potentials, where CO oxidation would be possible. The average current efficiency for $CO_2$ formation in a cyclic scan is ca. 6.7%, with values of ca. 9 and 2% in the positive-going and negative-going scan, respectively (see Table 2). Finally, it should be noted that there are no significant differences in the CVs between the first and second (subsequent) scan(s); the amount of $CO_2$ formation in the first positive-going scan, however, is lower than in the second scan, which is associated with the lower coverage of EG adsorbate formed in the low potential region. For the first positive-going scan, adsorbate formation occurs in the low potential region of that scan, while for the second and subsequent scan, adsorbate formation occurs in the low potential region of the preceding negative-going scan and during the positive-going scan.

Similar type CVs with a peak at around 0.7 V were reported by de Lima et al. for a Pt catalyst for dilute EG solution (0.1 M). For higher concentrations they found the maximum to shift to more positive values, and at concentrations $\geq$2 M it had moved outside the potential range (0.1–0.8 V) covered in those scans [15]. Likewise, Neto et al. found a continuous current increase with no pronounced maximum in measurements on a $Pt_{50}Ru_{50}$/Vulcan catalyst in 1.0 M EG up to 0.8 V [16].

In agreement with the observation of a rather low activity for EG decomposition (see Fig. 4), these observations indicate that at potentials with measurable rates the EG oxidation activity is not limited by $CO_{ad}$ poisoning, but rather by C–C bond breaking. Therefore, also on the PtRu/Vulcan catalyst electrode EG oxidation results predominantly in C2 by-product formation under current reaction conditions, and C–C bond breaking as well as $CO_2$ formation represent minority pathways. These observations agree even quantitatively with results reported by de Lima et al., who found a $CO_2$ yield of 8% after 6 min of EG electrolysis on $Pt_{62}Ru_{38}$ from IR spectroscopic measurements [15].

Comparing EG bulk oxidation (solid line, Fig. 11) with EG adsorbate oxidation (see dashed line in Fig. 11 for EG adsorbate stripping after adsorption at 0.26 V), we see that although the bulk oxidation current starts already at lower potential and is much larger than that of EG adsorbate oxidation, the onset potentials for $CO_2$ formation are identical for EG bulk oxidation and EG adsorbate oxidation. Furthermore, the $CO_2$ ion currents (solid line, Fig. 11b) are also nearly same in both cases. Hence, similar as for Pt/Vulcan, the total amount of $CO_2$ formed in the two cases is of comparable magnitude, suggesting that also on PtRu/Vulcan $CO_2$ formation during EG bulk oxidation (in potentiodynamic measurements) is largely caused by oxidation of $CO_{ad}$ formed during EG decomposition in the low potential region.

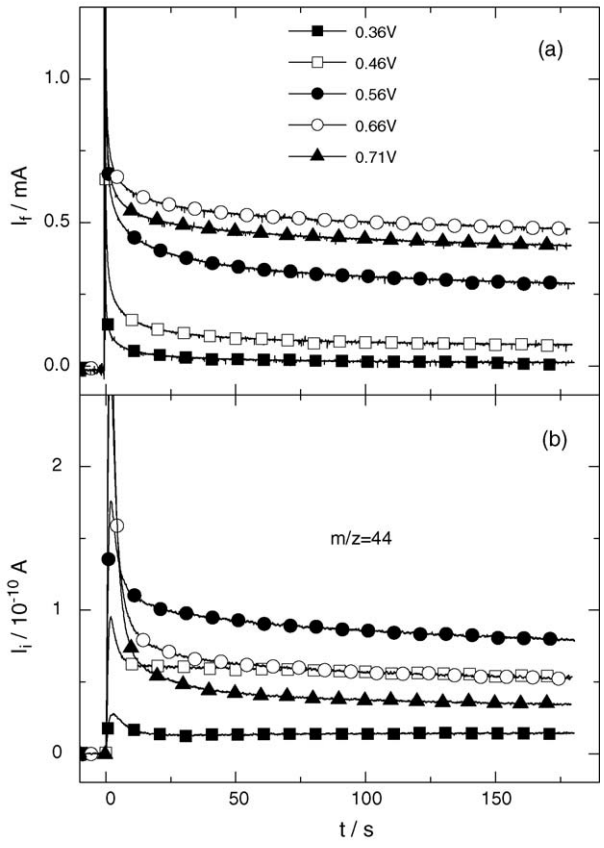


Fig. 12. Faradaic current (a) and the corresponding $m/z = 44$ ion current (b) transients after the potential step from 0.06 V to different reaction potentials on a PtRu/Vulcan catalyst electrode in 0.1 M ethylene glycol + 0.5 M $H_2SO_4$ solution (reaction potentials see figure).

The Faradaic current and $CO_2$ ion current transients obtained after a potential step from 0.06 V to different reaction potentials between 0.36 and 0.71 V in 0.1 M EG + 0.5 M $H_2SO_4$ solution are shown in Fig. 12. Similar to the procedure in the potential-step experiments on Pt/Vulcan catalyst the sample had been cleaned prior to the experiment by holding it at 0.9 V for 3 s and then stepping back to 0.06 V (time at 0.06 V: 30 s). In test measurements it was verified that this treatment had no significant effect on the electrochemical properties of the catalyst (Ru leaching), as evidenced by base CV measurements. The general characteristics of the resulting transients closely resemble those described above for EG oxidation on Pt/Vulcan. The Faradaic currents first pass through an initial current spike and then level off towards their steady-state values, which are approximately reached during the time of the measurements (3 min). The steady-state current values increase with higher reaction potential up to 0.66 V, while at the highest reaction potential (0.71 V) it decreases again. The $CO_2$ ion current signals equally pass through an initial maximum and then decay to their steady-state value. In this case we did not observe a second weak maximum in the $CO_2$ ion current signal, as it was detected for EG oxidation on Pt/Vulcan at medium potentials, indicating that for PtRu/Vulcan the same process, most likely C–C bond breaking, is rate limiting for $CO_2$ formation over the entire potential regime evaluated.

The initial maximum in $CO_2$ formation, which is less pronounced than that of the Faradaic current, but stronger than on the Pt/Vulcan catalyst, indicates that also in this case the Faradaic current spike is not entirely due to double-layer charging. Hence, also for PtRu/Vulcan the initial oxidation reaction, on the adsorbate free catalyst, is faster than that on the partly adsorbate covered surface under steady-state conditions. Similar to Pt/Vulcan the steady-state $CO_2$ ion current equally increases with higher reaction potential, but in this case the maximum current is reached at 0.56 V. Higher reaction potentials cause the steady-state $CO_2$ ion current to decrease.

The final Faradaic and ion current values within the measurement period of ca. 3 min are used to calculate the quasi steady-state current efficiencies for $CO_2$ formation at the different reaction potentials, which are plotted again in Fig. 10. Remarkably, the current efficiency for $CO_2$ formation decreases steadily with increasing reaction potential, from 11% at 0.36 V to 0.8% at 0.71 V. Therefore, the comparable values of the average current efficiencies for $CO_2$ formation on the Pt/Vulcan and PtRu/Vulcan catalysts, which were obtained by integrating over the CVs, result from a very different potential dependence, with a weak increase with potential for the Pt/Vulcan catalyst compared to a pronounced decay with potential for the PtRu/Vulcan catalyst. This behavior can be explained by a combination of two effects (i) by the much higher activity of PtRu/Vulcan for $CO_{ad}$ oxidation at lower potentials, so that even under these conditions, which seem to be favorable for C–C bond breaking, $CO_2$ formation is possible [47,48] and (ii) by a decrease in C–C bond breaking activity with increasing potential, which can be tentatively explained by the more pronounced $OH_{ad}$ formation on the catalyst compared to Pt/Vulcan. For practical applications it is important to note, however, that despite of the higher $CO_2$ current efficiency of the PtRu/Vulcan catalyst at low potentials, compared to Pt/Vulcan, the total current obtained on this catalyst in the potential range up to 0.5 V is still low, albeit significantly higher than on Pt/Vulcan. At 0.5 V both Faradaic current and $CO_2$ current efficiency of the two catalysts, Pt/Vulcan and PtRu/Vulcan, are of similar magnitude, at higher (but technically little relevant) potentials Pt/Vulcan is the better, more active and more selective catalyst.

### 3.2.3. Ethylene glycol oxidation on $Pt_3Sn$/Vulcan

Similar to the Pt/Vulcan and PtRu/Vulcan catalysts we equally characterized the activity of the $Pt_3Sn$/Vulcan for EG oxidation and their selectivity for complete oxidation to $CO_2$ by cyclic voltammetry and by potential-step oxidation transients. A set of cyclic voltammograms (CVs) and corresponding mass spectrometric cyclic voltammograms (MSCVs) is shown in Fig. 13. In order to prevent Sn dissolution, the upper potential limit was lowered to 0.61 V [43]. Therefore the CVs do not show the entire range of the main oxidation peak, but only their ascending signal at the low potential side. Again the respective curves for EG adsorbate stripping (Fig. 13, dashed line, after EG adsorption at 360 mV) and for EG bulk oxidation on the Pt/Vulcan catalyst (Fig. 13, dotted line) as well as the contribution from $CO_2$ formation to the Faradaic current (Fig. 13, dash-dotted line) are included in the CV and MSCV for comparison.

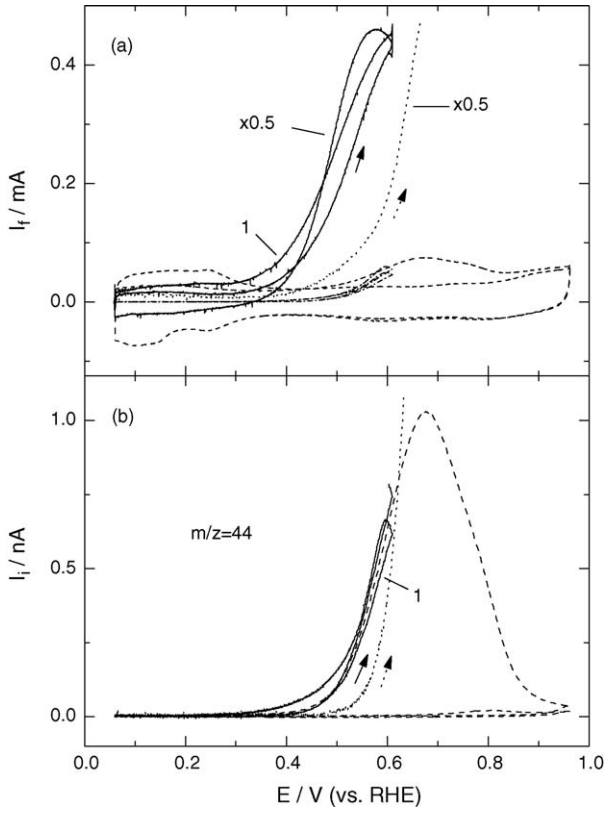


Fig. 13. Simultaneously recorded CVs (a) and $m/z = 44$ MSCVs (b) on a $Pt_3Sn$/Vulcan catalyst electrode in 0.1 M ethylene glycol + 0.5 M $H_2SO_4$ solution (full lines); dashed line: oxidative stripping of the ethylene glycol adsorbate formed at 0.36 V (full cycle). For comparison, the signals for ethylene glycol bulk oxidation on the Pt/Vulcan catalyst electrode are also shown (dotted lines). The calculated contribution of $CO_2$ formation to the Faradaic current signal is indicated by the dash-dotted line (scan rate: 10 mV $s^{-1}$).

The current peak for ethylene glycol oxidation on the $Pt_3Sn$/Vulcan catalyst electrode starts at around 0.3 V (Fig. 13a, solid line), which is 50 mV more negative than on the Pt/Vulcan electrode, while the onset potential for $CO_2$ formation is around 0.4 V (Fig. 13b, solid line), which is about 100 mV more negative than the onset potential on Pt/Vulcan (Fig. 8b, solid line) and about 50 mV more positive than that on PtRu/Vulcan catalyst electrodes (Fig. 11b, solid line). In the negative-going scan both the Faradaic current signal and the mass spectrometric current first increase slightly and then decay, after passing through a maximum. Comparison with the EG adsorbate stripping signal on the $Pt_3Sn$/Vulcan catalyst electrode (Fig. 13, dashed lines) shows directly that this maximum is not identical with the peak maximum that would have been observed when scanning to more positive potentials, but results from an increase in rate after reversing the potential scan. The decaying signal in the negative-going scan then largely follows that in the positive-going scan, but at slightly more negative potentials.

Although the actual peak maximum was not reached because of the low potential limit, the maximum Faradaic current value of about 0.9 mA is not far from the maximum current obtained on Pt/Vulcan at much higher potential (1.1 mA at 0.66 V). In the second and following positive-going scans the Faradaic currents are slightly lower than in the first scan; in contrast to the slightly

higher $CO_2$ ion currents. The onset for $CO_2$ formation does not shift. The increase in $CO_2$ formation for subsequent scans is tentatively associated with the increasing $CO_{ad}$ coverage, due to the longer time of dissociative adsorption of EG in the low potential region in the negative- and positive-going scan.

The current contribution from $CO_2$ formation on the $Pt_3Sn$/Vulcan catalyst electrode is indicated again by the dash-dotted line in Fig. 13a. Also in this case it is very low, but different from the behavior of the PtRu/Vulcan catalyst it is almost identical in the positive-going and in the negative-going scan. Similar to Pt/Vulcan (Fig. 13, dotted line) there is no significant $CO_2$ formation in the low potential regime below 0.3 V on the $Pt_3Sn$/Vulcan catalyst. The signal for $CO_2$ formation is actually shifted by 20 mV to more positive potentials compared to the Faradaic current signal, which corresponds to a shift by 40 mV compared to what would be expected when considering the delay between Faradaic current signal and mass spectrometric signal (ca. 1 s). Apparently, in this case $CO_2$ formation does not fully coincide with the increase in the total EG oxidation rate. The mean current efficiency for $CO_2$ formation, integrated over the complete potential cycle, is around 4%, and similar values were obtained also for the positive-going and negative-going scan separately (see Table 2). Hence, also for the $Pt_3Sn$/Vulcan catalyst complete oxidation is a minority reaction pathway, and ethylene glycol oxidation results predominantly in C2 reaction by-products.

Comparing the bulk oxidation signal (Fig. 13, solid line) with that for EG adsorbate stripping on $Pt_3Sn$/Vulcan (Fig. 13, dashed line), we see that although the bulk oxidation current starts already at lower potential and is much larger than that for EG adsorbate oxidation (Fig. 13a), the onset potentials for $CO_2$ formation (Fig. 13b, full line) are practically the same in both cases, and the same holds true also for the $CO_2$ ion currents at potentials $\leq$0.61 V. Based on this comparison it is very likely that in the positive-going scan the $CO_{ad}$ formed by EG dissociation in the low potential region is not completely oxidized up to the potential limit of 0.61 V, so that the $CO_2$ formation rate can even increase for a short time after reversing the potential scan. The same must be true also for the partial oxidation reactions leading to different C2 molecules, which comprise the dominant contribution to the EG oxidation current.

Faradaic current transients and $m/z = 44$ mass spectrometric ion current transients after a potential step from 0.06 V to different reaction potentials on the $Pt_3Sn$/Vulcan catalyst electrode between 0.46 and 0.56 V in 0.1 M EG + 0.5 M $H_2SO_4$ solution are displayed in Fig. 14. In this case the catalyst pretreatment, prior to the potential step, was somewhat different than that for the other two catalysts. Before the potential step, the $Pt_3Sn$/Vulcan was scanned in EG containing solution between 0.06 and 0.61 V for three times at a scan rate of 10 mV $s^{-1}$, therefore the catalyst surface contains an unknown amount of $CO_{ad}$. Nevertheless, also for this catalyst we find an initial current spike both in the Faradaic current and in the $CO_2$ ion current signal, indicating that the Faradaic current spike does not only result from double-layer charging, but contains contributions also from the EG oxidation reaction and $CO_{ad}$ oxidation. For the $CO_2$ ion current the initial spike increases with higher reaction

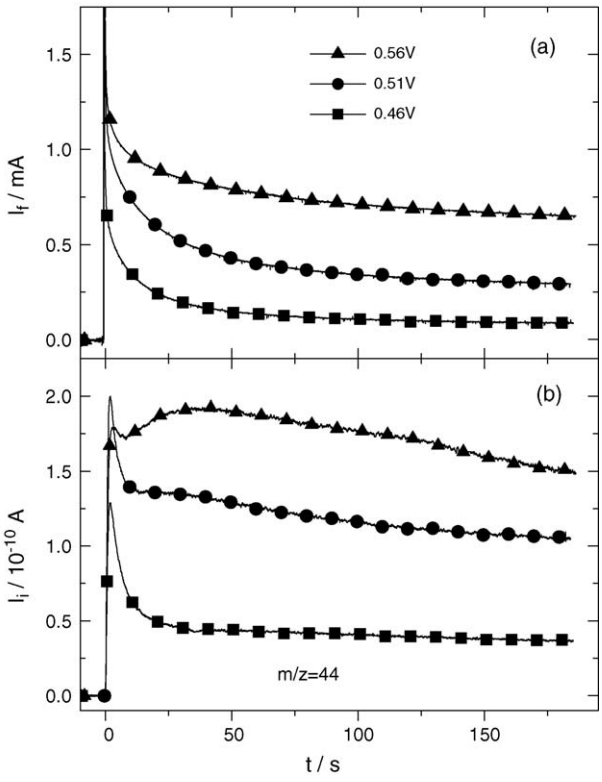


Fig. 14. Faradic current (a) and corresponding ion current of $m/z = 44$ (b) transients after the potential step from 0.06 V to different potentials on the $Pt_3Sn$/Vulcan catalyst electrode in 0.1 M ethylene glycol + 0.5 M $H_2SO_4$ (reaction potentials see figure).

potential, but only on an absolute scale. Comparing it with the steady-state current of the $CO_2$ signal its contribution becomes increasingly less, and it is almost completely disappeared at 0.56 V reaction potential. At this potential we also find a pronounced maximum in the $CO_2$ ion current after about 30 s, which starts to develop already at 0.51 V reaction potential. Such kind of maxima are well known for $CO_{ad}$ oxidation transients and are generally attributed to a nucleation and growth mechanism.

The steady-state values of the Faradaic current, the $m/z = 44$ ion current, and the $CO_2$ current efficiency for the different reaction potentials, determined after 3 min reaction time, are plotted in Fig. 10. The current efficiency for $CO_2$ formation decreases from 3.1 to 1.6% for increasing the reaction potential from 0.46 to 0.56 V. At potentials between 0.51 and 0.56 V the oxidative current on the $Pt_3Sn$/Vulcan catalyst electrode is the highest among the three catalysts. The current efficiency for $CO_2$ formation, however, is only ca. 2%.

In total, Sn was found to mainly promote the partial oxidation of EG to the C2 reaction intermediates. In addition, in agreement with earlier findings [38,40,42,43], it can also enhance the rate of $CO_2$ formation via $CO_{ad}$ oxidation (Fig. 7). On the other hand, it hinders the C–C bond breaking process or, more precisely, the dissociation of EG to $CO_{ad}$ (Figs. 6 and 7), at least on a relative scale, relative to the total oxidation rate. These observations closely resemble previous findings for the oxidation of other C2 molecules, ethanol and acetaldehyde, where the presence of Sn significantly enhances the total oxidation rate, but reduces the

amount of complete oxidation to $CO_2$ [27,49,50]. The (relative) decay in $CO_2$ formation can be tentatively explained by a geometric ensemble effect, assuming that larger Pt ensembles are required for C–C bond breaking than for partial oxidation of these C2 molecules. This picture does not explain, however, the increase in total oxidation rate, despite of the decrease in the number of Pt sites in the $Pt_3Sn$ alloy particles compared to Pt. Other effects, such as an electronic modification of the Pt or the classic bifunctional mechanism [48], must be involved as well. Sn certainly helps to remove adsorbed CO from the surface and this way enhance the availability of free Pt sites, e.g., for partial oxidation of EG to C2 side products, but it is not clear so far, whether this is the dominant effect.

## 4. Ethylene glycol oxidation in direct oxidation fuel cell applications

Finally it has to be noted that for all three catalyst the mass normalized EG oxidation rates and hence the current densities are too low for technical applications: from the maximum Faradaic current of $\leq$0.3 mA at 0.5 V and per 8 μg metal loading ($Pt_3Sn$/Vulcan) we can extrapolate a kinetic limit of 0.22 A per 5 mg metal content under these conditions, equivalent to a limiting anode current density of 0.22 A $cm^{-2}$ for 5 mg $cm^{-2}$ metal loading. More important, the very high amounts of toxic by-products (>90%), due to incomplete oxidation of the EG feed, presently exclude its use in direct oxidation fuel cells, at least for room temperature operation. Significant improvements in the C–C bond breaking activity appear to be more crucial than an overall enhancement of the EG oxidation activity. This involves (i) elevated reaction temperatures in order to activate the C–C bond breaking step, (ii) the introduction of other alloy components, and (iii) the optimization of the operating conditions in order to minimize the content of toxic partial oxidation products in the exhaust. Further quantitative studies on these aspects are planned.

## 5. Conclusions

Investigating the interaction of ethylene glycol with realistic, carbon supported Pt, PtRu and $Pt_3Sn$ catalysts by combined electrochemical and quantitative on-line DEMS measurements under fuel cell relevant conditions, i.e., under continuous reaction and continuous electrolyte flow conditions, we could demonstrate that

(i) dissociative ethylene glycol adsorption is inhibited on all three catalyst electrodes by adsorbed hydrogen at the most cathodic potential (0.06 V), but becomes more facile with increasing potentials, until the steady-state adsorbate coverage is reduced again by the onset of adsorbate oxidation;
(ii) on all three catalysts $CO_{ad}$ represents the dominant stable adsorbed species formed upon EG decomposition, with the maximum coverage obtained after 300 s EG adsorption decaying from Pt/Vulcan ($\theta_{CO,max} = 0.6$ $\theta_{CO,sat}$ 0.4 V) via $Pt_3Sn$/Vulcan (($\theta_{CO,max} = 0.4$ $\theta_{CO,sat}$ at 0.35 V) to PtRu/Vulcan ($\theta_{CO,max} = 0.2$ $\theta_{CO,sat}$ at 0.2 V));
(iii) both on a bare catalyst surface as well as under steady-state conditions complete oxidation to $CO_2$ is a minority reaction pathway (<6% at relevant currents), formation of incompletely oxidized C2 molecules prevails (contributions from partial oxidation C1 products (formaldehyde, formic acid) are possible), indicating that C–C bond breaking is slow and rate limiting for $CO_2$ formation;
(iv) the amount of $CO_2$ formation during the reaction depends on two factors, the activity for C–C bond breaking and the activity for $CO_{ad}$ oxidation, which can, depending on the potential dependence of these rates, result in different characteristics for the potential dependent amount of $CO_2$ formation;
(v) EG oxidation is possible also at potentials below the onset of $CO_2$ formation, where partly oxidized C2 (and possibly C1) species represent the only reaction product;
(vi) the addition of Ru or Sn increases the activity for EG oxidation in the low potential regime (around 0.4–0.5 V), and also lowers the onset potential for $CO_2$ formation, but on the other hand lowers the selectivity for $CO_2$ formation in the high potential region, which is attributed to a reduced activity for C–C bond breaking.

The data are consistent with the parallel reaction pathway mechanism proposed in earlier studies, with $CO_2$ formation via C–C bond breaking, $CO_{ad}$ formation and oxidation of the resulting $CO_{ad}$ in the one pathway and partial oxidation of ethylene glycol to higher oxidized C2 species such as glycol aldehyde, glycolic acid, etc., which leave the catalyst as soluble by-products, in the other pathway. Furthermore, they clearly show that under present reaction condition both the low kinetic limit for the EG oxidation activity ($\leq$0.22 A $cm^{-2}$ at 5 mg $cm^{-2}$ metal loading) and in particular the high emission of toxic by-products under steady-state conditions rule out technical applications of this reaction in a direct oxidation fuel cell. The influence of elevated operation temperatures and other alloy components on the reaction characteristics needs to be investigated.

## Acknowledgements

We gratefully acknowledge financial support by the Foundation "Landesstiftung Baden-Württemberg" (programme 'Portable Mini Fuel Cells') and by the Deutsche Forschungsgemeinschaft (Be 1201/12-1) as well as support for the visit of Y.Z. by the Ministry of Education of the People's Republic of China (MoE) and by the Deutsche Forschungsgemeinschaft.

## References

[1] F. Kadirgan, B. Beden, C. Lamy, J. Electroanal. Chem. 136 (1982) 119.
[2] G. Horanyi, V.E. Kazarinov, Y.B. Vassiliev, A. Andreev, J. Electroanal. Chem. 147 (1983) 263.
[3] F. Hahn, B. Beden, F. Kadirgan, C. Lamy, J. Electroanal. Chem. 216 (1987) 169.
[4] L.-W.H. Leung, M.J. Weaver, J. Phys. Chem. 92 (1988) 4019.
[5] P.A. Christensen, A. Hamnett, J. Electroanal. Chem. 260 (1989) 347.

[6] J.M. Orts, A. Fernandez-Vega, J.M. Feliu, A. Aldaz, J. Clavilier, J. Electroanal. Chem. 290 (1990) 119.
[7] L.-W.H. Leung, M.J. Weaver, Langmuir 6 (1990) 323.
[8] E.M. Belgsir, E. Bouhier, H.E. Yei, K.B. Kokoh, B. Beden, H. Huser, J.M. Leger, Electrochim. Acta 36 (1991) 1157.
[9] S.-G. Sun, A.-C. Chen, T.-S. Huang, J.-B. Li, Z.-W. Tian, J. Electroanal. Chem. 340 (1992) 213.
[10] B. Wieland, J.P. Lancaster, C.S. Hoaglund, P. Holota, W.J. Tornquist, Langmuir 12 (1996) 2594.
[11] J.F.E. Gootzen, W. Visscher, J.A.R. Van Veen, Langmuir 12 (1996) 5076.
[12] M. Betowska-Brzezinska, T. Uczak, R. Holze, J. Appl. Electrochem. 27 (1997) 999.
[13] A. Dailey, J. Shin, C. Korzeniewski, Electrochim. Acta 44 (1998) 1147.
[14] A. Kelaidopoulou, G. Kokkinidis, A. Milchev, J. Electroanal. Chem. 444 (1998) 195.
[15] R.B. de Lima, V. Paganin, T. Iwasita, W. Vielstich, Electrochim. Acta 49 (2003) 85.
[16] A.O. Neto, T.R.R. Vasconcelos, R.W.R.V. da Silva, M. Linardi, E.V. Spinace, J. Appl. Electrochem. 35 (2005) 193.
[17] W. Hauffe, J. Heitbaum, Electrochim. Acta 23 (1978) 299.
[18] B. Beden, F. Kadirgan, A. Kahyaoglu, C. Lamy, J. Electroanal. Chem. 135 (1982) 329.
[19] F. Kadirgan, B. Beden, C. Lamy, J. Electroanal. Chem. 143 (1983) 135.
[20] F. Kadirgan, E. Bouhier-Charbonnier, C. Lamy, J.M. Leger, B. Beden, J. Electroanal. Chem. 286 (1990) 41.
[21] S.-C. Chang, Y. Ho, M.J. Weaver, J. Am. Chem. Soc. 113 (1991) 9506.
[22] N.M. Markovic, M.L. Avramov-Ivic, N.S. Marinkovic, R.R. Adzic, J. Electroanal. Chem. 312 (1991) 115.
[23] E. Peled, T. Duvdevani, A. Ahron, A. Melman, Electrochem. Sol. Lett. 4 (2001) A38.
[24] E. Peled, V. Livshits, T. Duvdevani, J. Power Sources 106 (2002) 245.
[25] H. Wang, Z. Jusys, R.J. Behm, Fuel Cells 4 (2004) 113.
[26] H. Wang, Z. Jusys, R.J. Behm, J. Phys. Chem. B 108 (2004).
[27] H. Wang, Z. Jusys, R.J. Behm, J. Power Sources, in press.
[28] T.J. Schmidt, H.A. Gasteiger, G.D. Stäb, P.M. Urban, D.M. Kolb, R.J. Behm, J. Electrochem. Soc. 145 (1998) 2354.
[29] T.J. Schmidt, H.A. Gasteiger, R.J. Behm, J. Electrochem. Soc. 146 (1999) 1296.
[30] Z. Jusys, R.J. Behm, J. Phys. Chem. B 105 (2001) 10874.
[31] Z. Jusys, J. Kaiser, R.J. Behm, Phys. Chem. Chem. Phys. 3 (2001) 4650.
[32] H. Baltruschat, Interfacial Electrochemistry—Theory, Experiment and Applications, Marcel Dekker, Inc., New York, 1999, pp. 577–597.
[33] Z. Jusys, H. Massong, H. Baltruschat, J. Electrochem. Soc. 146 (1999) 1093.
[34] H. Baltruschat, U. Schmiemann, Ber. Bunsenges. Phys. Chem. 97 (1993) 452.
[35] H.A. Gasteiger, N.M. Markovic, P.N. Ross, E.J. Cairns, J. Phys. Chem. 97 (1993) 12020.
[36] M. Watanabe, S. Motoo, J. Electroanal. Chem. 60 (1975) 275.
[37] Z. Jusys, J. Kaiser, R.J. Behm, Electrochim. Acta 47 (2002) 3693.
[38] M. Watanabe, M. Shibata, S. Motoo, J. Electroanal. Chem. 187 (1985) 161.
[39] H.A. Gasteiger, N. Markovic, P.N. Ross, E.J. Cairns, J. Phys. Chem. 98 (1994) 617.
[40] H.A. Gasteiger, N.M. Markovic, P.N. Ross, J. Phys. Chem. 99 (1995) 8945.
[41] T.J. Schmidt, M. Noeske, H.A. Gasteiger, R.J. Behm, P. Britz, W. Brijoux, H. Bönnemann, Langmuir 13 (1997) 2591.
[42] T.J. Schmidt, H.A. Gasteiger, R.J. Behm, J. New Mater. Electrochem. Syst. 2 (1999) 27.
[43] H. Massong, H. Wang, G. Samajeské, H. Baltruschat, Electrochim. Acta 46 (2000) 701.
[44] M. Watanabe, Y. Furuuchi, S. Motoo, J. Electroanal. Chem. 191 (1985) 367.
[45] H. Wang, Ch. Wingender, H. Baltruschat, M. Lopez, M.T. Reetz, J. Electroanal. Chem. 509 (2001) 163.
[46] Z. Jusys, J. Kaiser, R.J. Behm, Langmuir 19 (2003) 6759.
[47] A. Hamnett, Catal. Today 38 (1997) 445.
[48] M. Watanabe, S. Motoo, J. Electroanal. Chem. 60 (1975) 267.
[49] C. Lamy, S. Rousseau, E.M. Belgsir, C. Coutanceau, J.M. Leger, Electrochim. Acta 49 (2004) 3901.
[50] F. Vigier, C. Coutanceau, F. Hahn, E.M. Belgsir, C. Lamy, J. Electroanal. Chem. 563 (2004) 81.
[51] H. Wang, Z. Jusys, R.J. Behm, in press.